A Reaction Path Study of the Catalysis and Inhibition of the *Bacillus anthracis* CapD γ-Glutamyl Transpeptidase
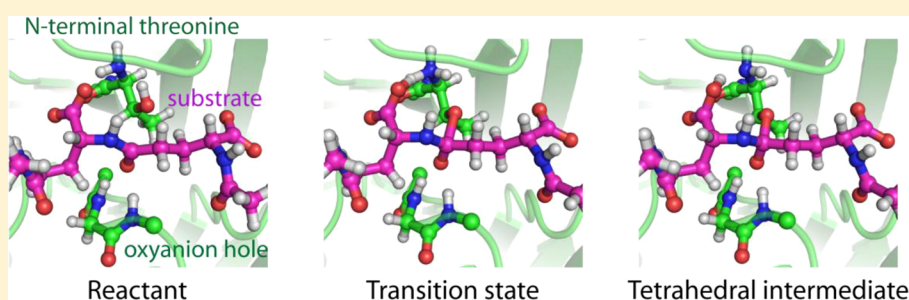
Ilja V. Khavrutskii,*,[†] Patricia M. Legler,[‡] Arthur M. Friedlander,[§] and Anders Wallqvist[†]

[†]Department of Defense Biotechnology High Performance Computing Software Applications Institute, Telemedicine and Advanced Technology Research Center, United States Army Medical Research and Materiel Command, Fort Detrick, Maryland 21702, United States

[‡]Center of Biomolecular Science and Engineering, Naval Research Laboratories, Washington, D.C. 20375, United States

[§]United States Army Medical Research Institute of Infectious Diseases, Fort Detrick, Maryland 21702, United States

ⓢ *Supporting Information*

N-terminal threonine
substrate
oxyanion hole
Reactant — Transition state — Tetrahedral intermediate

ABSTRACT: The CapD enzyme of *Bacillus anthracis* is a γ-glutamyl transpeptidase from the N-terminal nucleophile hydrolase superfamily that covalently anchors the poly-γ-D-glutamic acid (pDGA) capsule to the peptidoglycan. The capsule hinders phagocytosis of *B. anthracis* by host cells and is essential for virulence. The role CapD plays in capsule anchoring and remodeling makes the enzyme a promising target for anthrax medical countermeasures. Although the structure of CapD is known, and a covalent inhibitor, capsidin, has been identified, the mechanisms of CapD catalysis and inhibition are poorly understood. Here, we used a computational approach to map out the reaction steps involved in CapD catalysis and inhibition. We found that the rate-limiting step of either CapD catalysis or inhibition was a concerted asynchronous formation of the tetrahedral intermediate with a barrier of 22−23 kcal/mol. However, the mechanisms of these reactions differed for the two amides. The formation of the tetrahedral intermediate with pDGA was substrate-assisted with two proton transfers. In contrast, capsidin formed the tetrahedral intermediate in a conventional way with one proton transfer. Interestingly, capsidin coupled a conformational change in the catalytic residue of the tetrahedral intermediate to stretching of the scissile amide bond. Furthermore, capsidin took advantage of iminol−amide tautomerism of its diacetamide moiety to convert the tetrahedral intermediate to the acetylated CapD. As evidence of the promiscuous nature of CapD, the enzyme cleaved the amide bond of capsidin by attacking it on the opposite side compared to pDGA.

Bacillus anthracis is a Gram-positive, sporulating bacterium that normally resides in soil. The dormant spore form of the bacterium enters the mammalian host to cause anthrax infection and can withstand harsh conditions for decades.[1] Humans can contract the infection by exposure to the spores cutaneously, by ingestion, or by inhalation.[2] Once inside the human host, the dormant spores germinate into a rod-shaped, vegetative form. The vegetative form of the bacterium envelops its surface with a peptidic capsule that is essential for virulence and helps it evade the host immune response.[1,3−8]

The capsule is comprised of poly-γ-D-glutamic acid (pDGA) molecules covalently anchored to peptidoglycan.[8,9] The genes responsible for production of the capsular material, its attachment, and remodeling are known as *cap* genes.[5,10] One of the enzymes encoded by the *cap* operon is called CapD and is a γ-glutamyl transpeptidase (GGT) of the N-terminal nucleophile (Ntn) hydrolase superfamily.[11,12]

The Ntn hydrolases undergo an internal bond scission that creates an N-terminal Cys, Ser, or Thr residue that is essential for catalytic activity. The side chain of the newly generated N-terminal residue acts as a nucleophile, while the N-terminal amine participates in general acid−base catalysis. Figure 1 shows the active site of CapD that has an N-terminal Thr residue. Other members of the Ntn hydrolase superfamily include cephalosporin acylase, aspartylglucosaminidase, penicillin G acylase, and the quorum-quenching *N*-acyl homoserine lactone acylase.[13−17]

Deletion of the CapD gene from the *cap* operon prevents covalent attachment of the capsular material to the
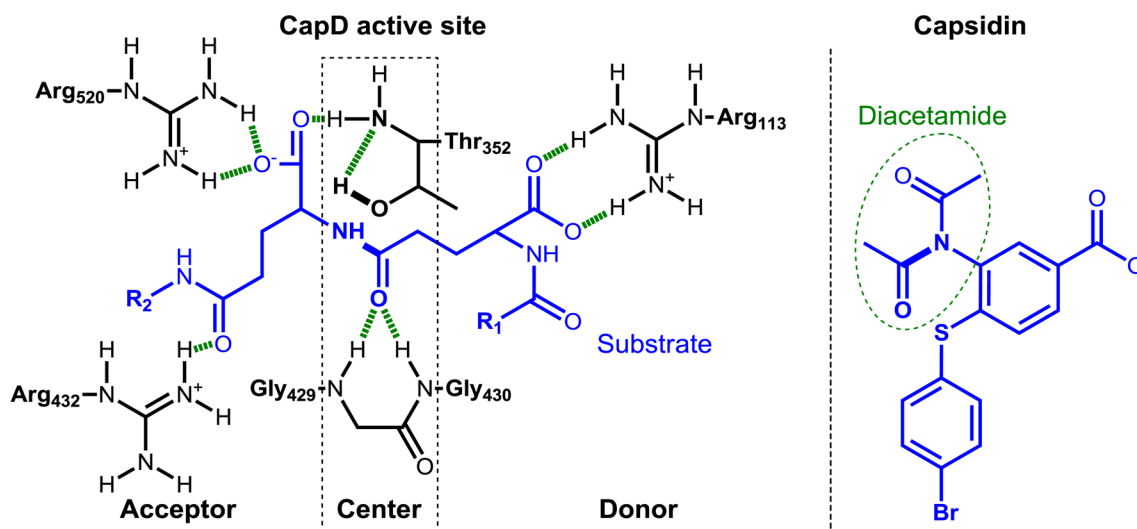
Figure 1. Active site of CapD with a poly-γ-D-glutamate substrate and the structure of the covalent inhibitor capsidin. The left panel shows a proposed binding mode for the natural poly-γ-D-glutamate substrate of CapD. Hydrogen bonds are depicted as green dashed lines. For this study, we used a di-γ-D-glutamate model with R_1 and R_2 being CH_3. The right panel shows capsidin, a covalent inhibitor of CapD that contains a reactive diacetamide group circled with a dashed line. The active site CapD residues are colored black, and the substrate or inhibitor is colored blue. The bonds that break during the catalysis are highlighted using bold solid lines.

peptidoglycan and enhances the susceptibility of the bacteria to phagocytosis by host macrophages[18] and neutrophils.[19] Consequently, recombinant CapD variants can be used as a therapeutic to break down the capsular material.[6,20−22] Alternatively, small-molecule inhibition of CapD may prevent the anchoring of the capsule.

Richter et al. recently discovered a covalent small-molecule inhibitor of CapD, named capsidin (see Figure 1).[10] In addition, they reported a number of capsidin variants that helped identify functional groups essential for inhibition.[10] Several mechanistic studies of related enzymes have been undertaken, but none have provided the details of CapD acylation by pDGA or rationalized the differences in CapD inhibition by capsidin and its variants.[14−17,23] Improving our understanding of these mechanisms may aid in the design and development of anti-infectives that prevent capsule anchoring by the CapD γ-glutamyl transpeptidase.

Critical for modeling efforts, CapD and several other members of the GGT family have been structurally characterized.[24−30] Figure 1 shows the active site of CapD divided into central, donor, and acceptor regions. The central region consists of the N-terminal catalytic Thr352 and oxyanion hole formed by the backbone NH groups of Gly429 and Gly430. Thr352 is the catalytic residue involved in the nucleophilic attack on the γ-peptide bond, whereas the oxyanion hole stabilizes the negative charge developing on the carbonyl oxygen of the scissile γ-peptide bond during the attack. The donor region of the active site contains Arg113 and Thr370, whereas the acceptor region contains Arg432 and Arg520. Thr352, Gly429, Gly430, Arg113, and Thr370 are highly conserved across the GGT family of Ntn-hydrolases.[11,30,31]

The first bound structure of CapD [Protein Data Bank (PDB) entry 3G9K] was determined with a di-α-L-Glu ligand.[29] The di-α-L-Glu ligand differs significantly from pDGA by the peptide linkage (α vs γ) and the chirality of the Glu (L vs D). These differences render the di-α-L-Glu ligand a poor mimic of pDGA. Interestingly, a related *Escherichia coli* GGT binds a single L-Glu by forming a salt bridge with the conserved Arg

residue in the donor region of the active site that is equivalent to Arg113 in CapD.[30] In contrast, the non-natural di-α-L-Glu ligand coordinates Arg520 and Arg432 within the acceptor region of the active site of CapD. Importantly, binding of the di-α-L-Glu to CapD appeared to be coupled to a change in the conformation of Arg520. A similar conformational change of Arg520 may accompany pDGA binding.

The role of Thr370 in the donor region of the active site is not completely understood. Mutational experiments demonstrated that Thr370 was critical for CapD catalysis,[29] like its counterparts in other GGTs.[28] The Thr370 counterparts appeared to hydrogen bond the N-terminal, catalytic threonine and were proposed to increase the nucleophilicity of the catalytic threonine,[30] mediate proton transfer from the -OH group to the -NH₂ group of the catalytic threonine,[27] and ensure that the N-terminal Thr assumed a catalytically competent conformation.[28] The proximity and high degree of conservation of Thr370 and its counterparts led to the proposal of a Thr-Thr catalytic dyad.[28]

In this paper, we studied the mechanism of CapD acylation by its native substrate pDGA and by the covalent inhibitor capsidin. Specifically, we applied docking[32] and reaction path optimization[33] on an ONIOM (our own N-layered integrated molecular orbital molecular mechanics)[34,35] hybrid quantum mechanical/molecular mechanical (QM/MM) potential energy surface.[36] With the help of these computational tools, we identified the rate-limiting step in CapD acylation as the formation of the tetrahedral intermediate.

The optimized reaction paths revealed important differences between pDGA and capsidin upon formation of tetrahedral intermediates with CapD. According to our models, the two molecules bound CapD with opposite orientations of the scissile bond in the active site. Thus, the prospective leaving group of pDGA was in the acceptor region, whereas that of capsidin was in the donor region of the active site. Furthermore, formation of the tetrahedral intermediate with pDGA was substrate-assisted and coupled to two proton transfers.[37] In contrast, formation of the tetrahedral intermediate with capsidin proceeded conventionally and involved
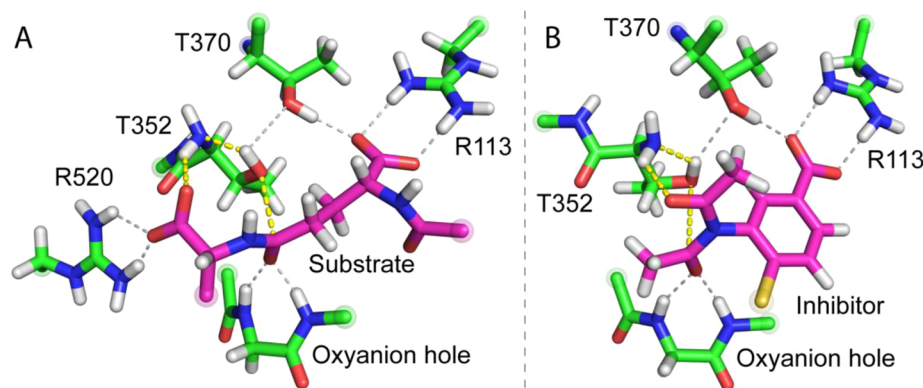
Figure 2. Quantum mechanical (QM) regions used in ONIOM(QM/MM) studies of CapD catalysis and inhibition. Atoms selected for the QM regions for the natural substrate model di-γ-D-glutamate (A) and covalent inhibitor capsidin (B) of CapD. Enzyme carbon atoms are colored green, while substrate and inhibitor carbon atoms are colored magenta. Hydrogen, nitrogen, oxygen, and sulfur atoms are colored white, blue, red, and yellow, respectively. Hydrogen bonds between the ligands and the enzyme are shown as dashed gray lines. Dashed yellow lines connect the atoms that are involved in the chemical transformations. Atoms that link the QM region to the rest of the system, described by molecular mechanics, are depicted with transparent spheres around them. These atoms are substituted for hydrogen atoms, and their bond lengths are adjusted accordingly during QM calculations.

only one proton transfer. Finally, the tetrahedral intermediate of capsidin was more stable than that of pDGA.

The mechanisms of the conversion of the tetrahedral intermediates of pDGA and capsidin to acylated CapD also differed. Capsidin underwent a conformational change coupled to an excessive stretching of the scissile amide bond. This unusual bond stretching was followed by a proton transfer, forming an iminol leaving group. Formation of the acetylated CapD with the iminol leaving group was possible because of the second acetyl group in the diacetamide moiety of capsidin (Figure 1). This finding rationalizes why capsidin variants with a single acetyl group fail to inhibit CapD.[10] In summary, this work provides mechanistic details of CapD catalysis and inhibition that offer useful insights into enzyme engineering and covalent inhibitor design.

METHODS

We generated the coordinates of the CapD complexes as described in the Supporting Information. The GaussView 5[38] graphical user interface was used to partition the system into QM and MM regions and to prepare the corresponding ONIOM(QM/MM) input files. Figure 2 shows our choices of the QM regions for pDGA and capsidin that incorporate the essential parts of the CapD active site, its substrate, or its inhibitor. For the complex with pDGA, the full system consisted of 7351 atoms with a net positive charge of nine, whereas the QM region included 95 atoms with a net charge of zero. For the complex with capsidin, the full system consisted of 7346 atoms with a net positive charge of 10. The QM region was slightly smaller and did not include Arg520 from the acceptor region of the active site. The total number of atoms of the QM region with capsidin was 82 with a net charge of zero.

All required MM parameters[39] were generated for the reactant states of both systems with the help of Antechamber from Amber Tools[40,41] and converted to the format required by Gaussian 09 (G09) software.[42] We generated and optimized reaction paths using the Conjugate Gradient Harmonic Fourier Beads (CG-HFB) method.[33] To generate smooth initial reaction paths, we performed a number of individual optimizations with progressive distance restraints[33] to push the reactant states of both systems toward the tetrahedral

intermediates and then toward the acylated enzymes. The adaptive positional restraints, with a force constant of 50.0 kcal mol^{-1} Å^{-2} on all of the atoms of the system, were enforced during those explorations to prevent unproductive conformational changes that were orthogonal to the reaction but could cause discontinuities in the potential energy profiles.[33] These positional restraints turned the rugged potential energy surface of CapD into a funnel-like potential[43,44] that was easier to optimize.

The reaction path optimization protocol closely followed our previous report.[33] The structures along the path were aligned using the root-mean-square best-fitting procedure for the first 100 atoms of the system.[33] All of the atoms were optimized using adaptive positional restraints, with a force constant of 50.0 kcal mol^{-1} Å^{-2}. Atoms involved in the transitions were assigned additional positional restraints with a force constant of 500.0 kcal mol^{-1} Å^{-2}. The ONIOM(QM/MM) energy and gradient calculations to drive reaction path optimization with CG-HFB were obtained using G09 software with default options.[42] Initially, we used a semiempirical QM potential, i.e., Austin Model 1 (AM1),[45] mechanically embedded with an Amber[39] MM force field. The final results reported here were obtained using the B3LYP/6-31G(d) QM potential electronically embedded with the Amber[39] MM force field.[36,46,47] Consequently, the reported values include polarization of the QM region by the MM atoms of the system. The energies and structures of the transition states were extracted from the optimized reaction paths and corresponding integral energy profiles. The latter were reconstructed from the ONIOM(QM/MM) forces as described elsewhere.[33]

RESULTS AND DISCUSSION

Mechanism of CapD Catalysis. *Model of CapD Bound to pDGA.* A study of CapD catalysis required a structure of the enzyme in complex with a substrate. Because the crystal structure of the CapD enzyme bound to its natural substrate pDGA was not available, we derived a corresponding model computationally. The pDGA substrate was modeled as a capped di-γ-D-glutamate (diDGA) peptide. Hence, the diDGA contained three peptide bonds, two of which were made with capping groups, $CH_3C(O)$- and -$NHCH_3$. Docking of diDGA

into the CapD structure (PDB entry 3G9K[29]) identified two principal binding modes. These modes could be distinguished by considering which region of the active site (donor vs acceptor) will host the covalently attached γ-glutamyl moiety, and which will host the leaving group following the cleavage of the γ-peptide bond. Alternatively, we could distinguish the two poses by considering the face of the peptide bond that would be attacked by Thr352 (*Re* vs *Si*).[48−50] Thus, the *Si* binding mode positioned the γ-glutamyl into the acceptor region of the active site coordinated by Arg520 and Arg432, whereas the leaving group was bound to the donor region of the active site. In contrast, the *Re* binding mode positioned the γ-glutamyl group in the donor region of the pocket coordinated by Arg113, whereas the leaving group was bound to the acceptor region of the active site. Because the *Re* mode, schematically depicted in Figure 1, agreed with available structural data from related GGT enzymes,[24,26,30] we chose this mode in our study of CapD catalysis.

We examined the diDGA interactions in the central, donor, and acceptor regions of the CapD active site. Figure 3 shows that the N-terminal α-carboxyl of the diDGA substrate formed two hydrogen bonds with the conserved Arg113, and two additional hydrogen bonds with Thr370 and Thr409, in the
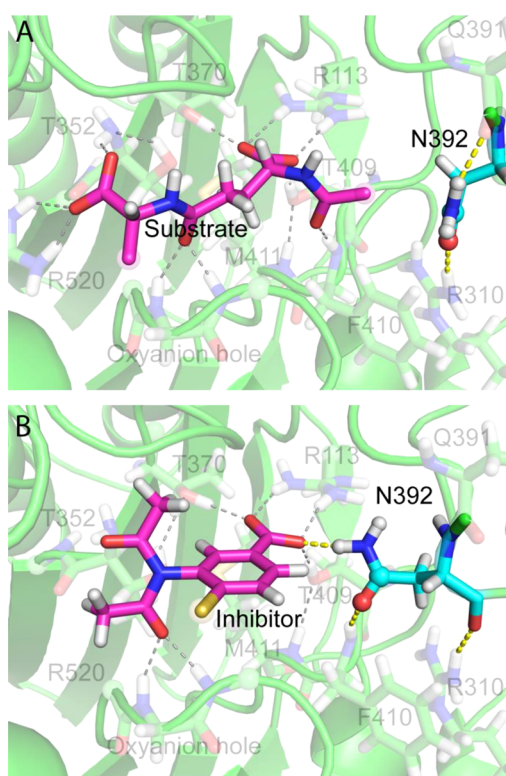

Figure 3. Models of CapD complexes with pDGA and capsidin. Optimized model structures of CapD in a complex with di-γ-D-glutamate (A) and covalent inhibitor capsidin (B). The enzyme cartoon representation and its carbon atoms are colored green; substrate and inhibitor carbon atoms are colored magenta, and carbon atoms of the flexible Asn392 are colored cyan. Hydrogen, nitrogen, oxygen, and sulfur atoms are colored white, blue, red, and yellow, respectively. Hydrogen bonds between the ligands and the enzyme are shown as dashed gray lines. Dashed yellow lines show hydrogen bonds that are affected by substrate and inhibitor binding. Atoms that link the QM region to the rest of the system, described by molecular mechanics, are depicted with transparent spheres around them.

donor region of the active site. To the best of our knowledge, participation of Thr370 in binding of the substrate has not been observed in other GGTs.[24,26,30] Interestingly, Thr370 did not form the expected hydrogen bonds with either the -NH₂ or -OH groups of the catalytic Thr352. The carbonyl oxygen of the N-terminal peptide bond formed a hydrogen bond with the backbone NH group of Phe410. The side chain of nearby Asn392 formed two hydrogen bonds: one between its carbonyl and the side chain of Arg310 and the other between its amide and the backbone carbonyl of Gln391.

In the central region of the active site, the carbonyl of the scissile γ-peptide bond coordinated the oxyanion hole via hydrogen bonding to the backbone NH groups of Gly429 and Gly430. In the acceptor region of the active site, the N-terminal NH₂ group of the catalytic Thr352 and the side chain of Arg520 coordinated the second α-carboxyl group that belonged to the leaving group of diDGA. The carbonyl oxygen of the third γ-peptide bond that was also part of the leaving group was involved in hydrogen bonding with Arg432. Importantly, the OH group of the catalytic Thr352 made an intramolecular hydrogen bond with the N-terminal NH₂ group, priming the substrate for a nucleophilic attack.

CapD Acylation Mechanism by pDGA. Our preliminary studies suggested that the CapD acylation reaction proceeded with the N-terminal amino group of Thr352 deprotonated. The protonated CapD would be able to execute acylation in only a single step, similar to the uncatalyzed acylation described elsewhere.[33] We found that such single-step acylation was associated with high barriers, regardless of the protonation state of the N-terminal amine of Thr352 (results not shown). Instead, CapD executed a more energetically favorable acylation by routing the reaction through a lower-energy metastable tetrahedral intermediate. This two-step reaction required the N-terminal amino group to be in a deprotonated state initially.

Formation of the Tetrahedral CapD Intermediate of pDGA. The energy profile in Figure 4 shows that the first step of CapD catalysis, i.e., formation of the tetrahedral intermediate, had a barrier of 22.3 kcal/mol. The energy of the tetrahedral intermediate was 18.0 kcal/mol, only 4.3 kcal/mol lower than that of the transition state (TS). This single catalytic step coupled two proton transfers to the formation of a bond between Thr352 and the substrate, namely Thr352(Oγ)−(C₂)diDGA.

Formation of the tetrahedral intermediate was initiated through the preparation for the transfer of a proton from Thr352(Oγ) to Thr352(N) by decreasing the Thr352(Oγ)−(C₂)diDGA and Thr352(Hγ)−(N)Thr352 distances from their initial values of 2.73 and 1.80 Å, respectively. Figure 4 shows the reaction energy profile from the initial reactant state R (marked with an arrow), through the TS, to the tetrahedral intermediate P, and Figure 5 shows the corresponding molecular structures. The first proton transfer was completed before the reaction reached the transition state and corresponded to a shoulder of ∼15 kcal/mol in the energy profile. At the end of the first proton transfer, the terminal α-amine of Thr352 briefly became protonated, yet the Thr352-(Oγ)−(C₂)diDGA bond did not completely form.

The proximal Thr370 appeared to assist in the first proton transfer by establishing a rather weak hydrogen bond to the transferring proton on the N-terminal amino group of the catalytic Thr352 residue at the transition state and product, but not on the -OH group of Thr352 at the reactant. Indeed, the Thr352(Hγ)−(Oγ)Thr370 distance was the shortest during the
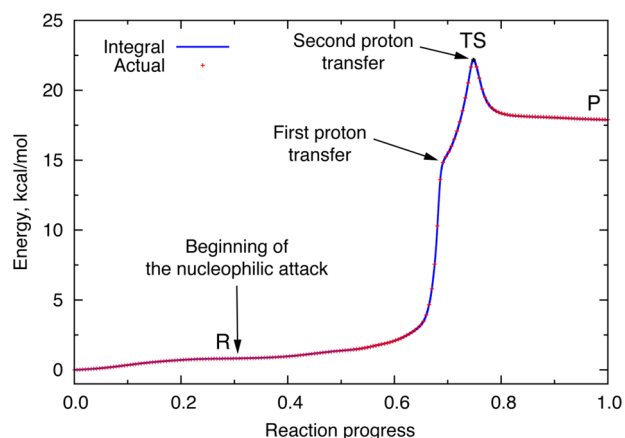
Figure 4. Energy profile for formation of the tetrahedral intermediate of CapD with di-γ-D-glutamate. The energy profile was calculated using the ONIOM[B3LYP/6-31G(d):Amber] potential with electronic embedding and is plotted along the reaction path that connects the reactant to the product (as parametrized using the reaction progress coordinate). The actual energy levels of the structural snapshots along the reaction are shown with red crosses. The matching integral energy is shown as a solid blue line and was derived from the corresponding forces. The transition state is denoted by a black cross and located atop the energy peak. Arrows indicate where the nucleophilic attack of CapD on di-γ-D-glutamate begins and where the two proton transfers occur along the reaction path. The total number of system snapshots used to generate the energy profile was 192. R, reactant; TS, transition state; P, product.

proton transfer. This was also reflected in the increase in the hydrogen bond length between Thr370 and the N-terminal α-carboxyl of diDGA. Note, however, that Thr370 did not directly participate in proton transfer, as was suggested for the related GGT of *E. coli*.[27] Interestingly, during the first proton transfer, the Thr352($C\alpha$–$C\beta$) bond stretched to 1.61 Å (compared to 1.56 and 1.58 Å in the reactant and product states, respectively), presumably to relieve conformational strain associated with the transfer.

The second proton transfer immediately followed the first one and coincided with the TS of the reaction. The second proton was transferred from the terminal α-amine of Thr352 to the α-carboxyl group of diDGA that is adjacent to the scissile peptide bond. At the TS shown in Figure 5, the distance between the proton and the nearest oxygen atom of the adjacent α-carboxyl group was 1.21 Å. The corresponding Thr352(N–H) bond was effectively broken at 1.30 Å. The Thr352($O\gamma$)–(C_2)diDGA distance reached 1.91 Å, whereas the C=O bond of the carbonyl group bound to the oxyanion hole was only slightly elongated from 1.25 to 1.27 Å.

The second proton transfer completed the formation of the metastable tetrahedral intermediate, labeled "P" in Figure 4. The bottom panel of Figure 5 shows the corresponding structural details of the tetrahedral intermediate. In the tetrahedral intermediate, the Thr352($O\gamma$)–(C_2)diDGA bond is completely formed at 1.56 Å. The C=O bond of the carbonyl group in the oxyanion hole stretched to 1.32 Å; i.e., the double bond transformed into a single bond with a partial negative charge on the oxygen atom.

The oxyanion hole strongly interacted with the diDGA substrate in the tetrahedral intermediate state. Indeed, the two hydrogen bonds with the oxyanion hole became stronger, as manifested by their contraction to 1.88 and 1.56 Å. In the reactant state, the corresponding distances were 2.00 and 1.72
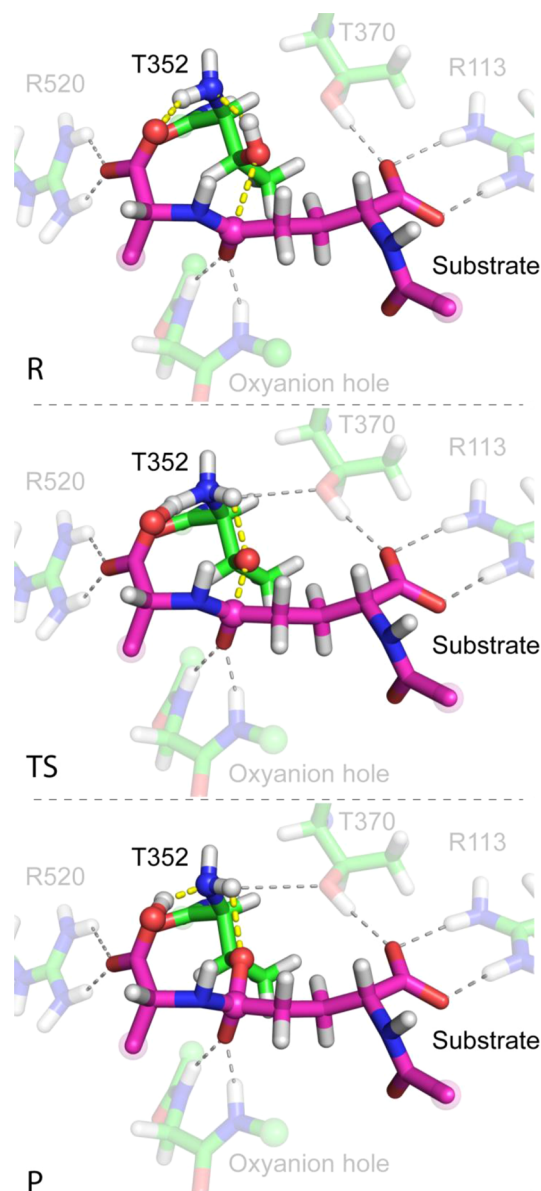

Figure 5. Reactant, transition state, and product for the formation of the tetrahedral intermediate of CapD with di-γ-D-glutamate. Snapshots show changes in the QM region of the ONIOM(QM/MM) system along the reaction path. Enzyme carbon atoms are colored green, while substrate carbon atoms are colored magenta. Hydrogen, nitrogen, and oxygen atoms are colored white, blue, and red, respectively. Hydrogen bonds between the ligands and the enzyme are shown as dashed gray lines. Dashed yellow lines connect the atoms that are involved in the chemical transformations. The residues of the active site that are not directly involved in the reaction are shown in faded, transparent colors. Atoms that link the QM region to the rest of the system described by molecular mechanics are depicted with transparent spheres around them. These atoms are substituted for hydrogen atoms, and their bond lengths are adjusted accordingly during QM calculations. R, reactant; TS, transition state; P, product.

Å, respectively, whereas in the TS, they were 1.93 and 1.64 Å, respectively. Nevertheless, as shown in Figure 4, the stabilization of the tetrahedral intermediate "P" was only 4.3 kcal/mol relative to the TS.

It appeared that CapD significantly destabilized the tetrahedral intermediate compared to Ntn-hydrolases such as aspartylglucosaminidase (AGA) and penicillin G acylase

(PGA).[15−17] Interestingly, a study of a model system derived from the PGA that employed the AM1 semiempirical potential reports the stabilization of a tetrahedral intermediate by only 2.6 kcal/mol.[14]

Overall, the formation of the tetrahedral intermediate was a double proton-coupled concerted asynchronous reaction. Furthermore, the discovered mechanism of CapD catalysis was substrate-assisted,[37] because the α-carboxyl group of diDGA adjacent to the scissile γ-peptide bond acted as the transient proton acceptor, just like the N-terminal α-amine of the catalytic Thr352. Indeed, Figure 5 shows that the α-amine of Thr352 relayed the proton from the OH group of Thr352 to the adjacent α-carboxyl group of diDGA and, thereby, remained deprotonated. Therefore, we would expect donor substrates lacking a carboxyl group that could interact with Arg520 and Thr352 and assist in catalysis to react with CapD more slowly.

It is worth noting that CapD could not cleave glutathione[9] or other GGT substrates, such as γ-glutamyl-anilides, under physiological conditions.[10,12] These GGT donor substrates lack the α-carboxyl groups of pDGA near the scissile amide bond. However, they also have the free N-terminal α-amine that pDGA does not have. The free α-amino group of typical GGT substrates can interfere with anchoring in the donor region of the CapD active site because, unlike typical GGTs, CapD has no carboxyl groups in the donor region of the active site that could stabilize the free α-amine. Therefore, the lack of CapD catalysis with regular GGT substrates could be due to either poor binding (free α-amine) or poor reactivity (lack of α-carboxyl). Answering these questions definitively would require additional experiments and/or calculations that gauge both binding and reactivity and are beyond the scope of this study.

In several QM studies, researchers have examined the reaction mechanism of acylation of Ntn-hydrolases using model systems in the gas phase; they report energy barriers in excess of 30 kcal/mol for the formation of the tetrahedral intermediate.[14−17] Like our work, these estimates represent enthalpic contributions to the barrier heights. To the best of our knowledge, this work is the first ONIOM(QM/MM) study of a threonine-based Ntn-hydrolase and provides a significantly lower estimate of the barrier height (22.3 kcal/mol for the formation of the tetrahedral intermediate). Note that our approach to finding transition states is known to overestimate barrier heights, suggesting that the actual barrier might be slightly lower.[33] Although still high, such reaction barrier heights have precedents in enzyme catalysis. For example, a glycogen phosphorylase enzyme has an activation energy of 21.2 kcal/mol,[51] with a corresponding free energy barrier of 15.2 kcal/mol when entropic effects are taken into consideration.[51]

Although it is generally considered that formation of the tetrahedral intermediate does not require a water molecule,[52] including water molecules might result in alternate pathways[15,53,54] with potentially lower activation energies. Finding such pathways is a challenging task in and of itself and was not attempted in this study.

Formation of the Acylated CapD Intermediate of pDGA. Formation of the γ-glutamylated CapD required complete scission of the γ-peptide bond of the diDGA substrate. This task, in turn, required a proton, which is generally thought to come directly from the protonated N-terminal α-amine of the catalytic Thr (Thr352 in CapD). However, CapD converted the tetrahedral intermediate into the acylated enzyme differently.

The observations that CapD did not significantly stabilize the tetrahedral intermediate, and that the proton resided on the α-carboxyl group of the substrate rather than on the N-terminal α-amino group of the enzyme, suggest that deprotonation by proton transfer to bulk water could provide additional stabilization of the tetrahedral intermediate. The proton necessary to cleave the γ-peptide bond could then come from the bulk water phase.

In the absence of water molecules, the only source of the proton in our model was the adjacent α-carboxyl of the substrate diDGA. Therefore, we studied the mechanism of transfer of a proton from the α-carboxyl to the nitrogen of the scissile γ-peptide bond of diDGA. The protonated α-carboxyl group of diDGA can relay the proton to the nitrogen of the scissile γ-peptide bond. Our hypothesis was that the barrier heights identified in this process would provide upper bounds for the final stage of CapD acylation.

Starting from the metastable, tetrahedral intermediate with a protonated second α-carboxyl group (shown as "P" in Figure 5), the proton reached the nitrogen on the scissile γ-peptide bond in four plausible steps, as detailed in the Supporting Information. Importantly, we estimated that none of the steps would have an activation barrier in excess of 10.0 kcal/mol, suggesting that the transfer of a proton from the α-carboxyl group of diDGA to the scissile amide bond is feasible even in the absence of water molecules.

Figure 6 shows the final product of the CapD acylation that contained the γ-glutamylated enzyme with the leaving group bound to the acceptor region of the active site. The relative positions of the α-carboxyl and γ-carbonyl groups changed
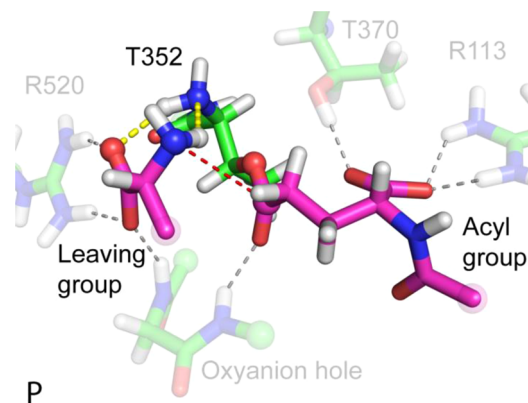

Figure 6. Final product of CapD acylation with di-γ-D-glutamate. The structure of the QM region of the ONIOM(QM/MM) system corresponded to the acylated CapD with the leaving group of di-γ-D-glutamate bound to the acceptor region of the active site. Enzyme carbon atoms are colored green, while carbon atoms of the substrate are colored magenta. Hydrogen, nitrogen, and oxygen atoms are colored white, blue, and red, respectively. Hydrogen bonds between the ligands and the enzyme are shown as dashed gray lines. Dashed yellow lines connect the atoms that are involved in the chemical transformations. These atoms are visually enhanced using solid spheres. The residues of the active site that are not directly involved in the reaction are shown in faded, transparent colors. Atoms that link the QM region to the rest of the system described by molecular mechanics are depicted with transparent spheres around them. These atoms are substituted for hydrogen atoms, and their bond lengths are adjusted accordingly during QM calculations. The dashed red line connects the atoms of the scissile γ-peptide bond of the substrate that has been cleaved.

dramatically following γ-peptide bond cleavage. In the acylated CapD, the adjacent α-carboxyl group bound one of the two NH prongs of the oxyanion hole as the carbonyl oxygen was pushed toward the donor region of the active site. In this configuration, the oxyanion hole coordinated one carboxyl and one acyl group. This demonstrated the ability of the two-pronged oxyanion hole to accommodate either one or two ligands.

The α-amino group of the newly formed leaving group of diDGA made a hydrogen bond with the N-terminal α-amine of Thr352, with both amino groups remaining deprotonated. Arg520 continued to coordinate the α-carboxyl of the leaving group. Considered in reverse order, this reaction would correspond to the transfer of an acyl group from the enzyme to the acceptor substrate. Therefore, acyl transfer during transpeptidation would have to overcome a barrier of at least 22.0 kcal/mol. During the transfer, α-amino groups of both the enzyme and the acceptor substrate would need to be deprotonated.

The requirement that α-amino groups of the acceptor substrate and of the catalytic Thr352 be deprotonated during transpeptidation is supported by recent studies of the pH dependence of the transpeptidation rate of a related GGT from *Bacillus subtilis*.[55,56] This bacterial GGT is similar to CapD in that it also lacks the lid loop and cleaves pDGA.[25,55] These studies found that the transpeptidation rate increased with increasing pH.

These observations allowed us to conclude that the rate of CapD acylation with the pDGA donor substrate will be limited by the formation of the tetrahedral intermediate with a barrier of 22.3 kcal/mol. Overall, CapD acylation was 3.4 kcal/mol endothermic.

Mechanism of CapD Inhibition with Capsidin. To study the mechanism of CapD inhibition by capsidin, we built the corresponding model complex, using the same procedure as described before. Below, we discuss the important structural features of the derived model, followed by the mechanism of inhibition of CapD.

Model of CapD Bound to Capsidin. The structure of the bound CapD complex with capsidin was derived like that of the complex with pDGA. However, to produce CapD-bound structures of capsidin that were compatible with the nucleophilic attack of Thr352, the two amide bonds of capsidin were allowed to rotate during docking. The four lowest-energy structures were compatible with covalent CapD inhibition and differed mostly in the position of the parabromothiophenol group of capsidin. We took the lowest-energy structure as the starting structure for our model of the complex depicted in Figure 3B.

According to our model (see Figure 3B), capsidin bound the active site of CapD in the central and donor regions of the active site. The only carboxyl group of capsidin interacted with Arg113 in the donor region of the active site, like the N-terminal α-carboxyl of diDGA. This carboxyl group is essential for CapD inhibition[10] and is equivalent to the N-terminal α-carboxyl group of diDGA. Asn392 changed its conformation to fill the void that in the case of diDGA was occupied by a carbonyl adjacent to the N-terminal carboxyl group shown in Figure 3A. The carbonyl of the Asn392 side chain anchored the backbone NH group of Phe410, so that the NH$_2$ group of Asn392 could form a hydrogen bond with the essential carboxyl group of capsidin.

In contrast to diDGA, the capsidin binding pose placed the *Si* face of the scissile peptide bond against the catalytic Thr352.

Thus, unlike with diDGA, the leaving group of the capsidin would be in the donor region of the active site and not in the acceptor region. This highlights the promiscuous nature of CapD with respect to inhibition by capsidin.

Unlike diDGA, capsidin did not engage either Arg520 or Arg432 in the acceptor region of the active site. However, capsidin made important interactions in the central region of the active site. In particular, the diacetamide group of capsidin shown in Figure 1 was configured such that one carbonyl bound the oxyanion hole while the other formed a hydrogen bond with the α-amino group of the N-terminal Thr352. With respect to the main benzene ring of capsidin, the carbonyl group of the acetyl that bound to the oxyanion hole was in the *cis* orientation, whereas the carbonyl of the other acetyl group was in the *trans* orientation. Finally, the parabromothiophenol group of capsidin protruded out of the active site without making any specific interactions.

The OH group of the catalytic Thr352 residue formed a 1.99 Å intramolecular hydrogen bond with the N-terminal α-amino group. The OH group also made a weaker hydrogen bond to the OH group of Thr370. The latter interaction was not observed with the diDGA substrate. The Thr352(Oγ)−(C)capsidin distance was relatively extended at 3.34 Å, while the carbonyl bond was 1.23 Å at the beginning of the reaction.

Mechanism of CapD Acylation by Capsidin. Following the arguments presented for the study of the mechanism of CapD catalysis, we kept the N-terminal α-amino group of the catalytic Thr352 deprotonated in the study of CapD inhibition.

Formation of the Tetrahedral CapD Intermediate of Capsidin. Figure 7 shows that the transition state to form the tetrahedral intermediate was 22.9 kcal/mol above the reactant. The tetrahedral intermediate product was 8.2 kcal/mol lower than the transition state, but 14.7 kcal/mol higher than the reactant. Compared to diDGA (see Figure 4), the tetrahedral intermediate of capsidin was significantly more stable.
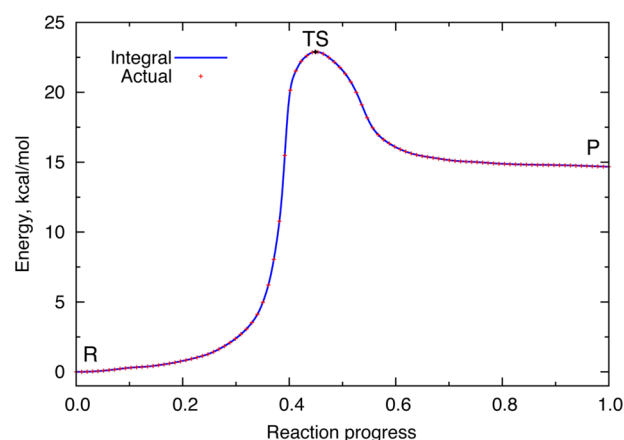

Figure 7. Energy profile for formation of the tetrahedral intermediate of CapD with covalent inhibitor capsidin. We calculated the energy profile using the ONIOM[B3LYP/6-31G(d):Amber] potential with electronic embedding and plotted it along the reaction path that connects the reactant to the product (as parametrized using the reaction progress coordinate). The actual energy levels of the structural snapshots along the reaction are shown with red crosses. The matching integral energy is shown as a solid blue line and was derived from the corresponding forces. The transition state is indicated as a black cross and located atop the energy peak. The total number of system snapshots used to generate the energy profile was 98. R, reactant; TS, transition state; P, product.

Formation of the tetrahedral intermediate between capsidin and CapD began with compression of the Thr352(Oγ)−(C)capsidin distance from 3.34 to 2.80 Å. Further compression from 2.80 to 2.60 Å initiated the transfer of the proton from Thr352(Oγ) to Thr352(N). Following the proton transfer, the Thr352(Oγ)−(C)capsidin bond was fully formed, reaching the anticipated length of 1.52 Å. The C=O bond of the carbonyl at the oxyanion hole was slightly elongated to 1.29 Å in the tetrahedral intermediate state.

Figure 8 shows that the proton transfer is complete at the transition state, with the Thr352(O)−(C)capsidin distance being 2.42 Å and the peptide bond length being 1.42 Å. The Thr352(O−H) distance was 1.93 Å (compared to 0.98 and 2.60 Å in the reactant and tetrahedral intermediate, respectively). The Thr352(Cα−Cβ) bond stretched during the proton transfer to 1.62 Å (compared to 1.55 and 1.58 Å in the reactant and product, respectively). The observed stretching of the Thr352(Cα−Cβ) bond was similar to that in the diDGA case and likely helped relieve the strain in the transiently formed five-member ring that included the Thr352-(Cα−Cβ) bond and the transferring proton.

The peptide bond that was under nucleophilic attack stretched from 1.40 to 1.56 Å. Interestingly, the other peptide bond that was not directly involved in the reaction shrank from 1.43 to 1.36 Å. Subsequently, the protonated NH$_3^+$ group of Thr352 rotated to establish hydrogen bonds with the OH group of Thr370 and the other carbonyl of the diacetamide moiety of capsidin. The corresponding distances changed from 2.58 Å to a more typical hydrogen bond distance of 1.87 Å, and from 2.21 to 1.66 Å.

In contrast to that of diDGA, the terminal α-amino group of Thr352 remained protonated in the tetrahedral intermediate of CapD with capsidin (Figure 8, bottom panel). Thus, only a single proton transfer was involved in the formation of the tetrahedral intermediate with capsidin, as opposed to two proton transfers as observed in the case of diDGA.

Formation of the Acetylated CapD Intermediate of Capsidin. Figure 9 shows that formation of the acetylated CapD from the tetrahedral intermediate of capsidin did not involve any productive steps with barriers higher than 2.5 kcal/mol. Therefore, formation of the tetrahedral intermediate was the rate-limiting step of CapD inhibition with capsidin. Nevertheless, the reaction mechanism of the formation of acetylated CapD from the tetrahedral intermediate was rather unexpected.

Figure 10 shows a conformational transition of the side chain of Thr352 that was coupled to the peptide bond cleavage and is the first step of the mechanism of formation of the acetylated CapD intermediate. This unusual conformational change rotated the Thr352 side chain about the Thr352(Cα−Cβ) bond by approximately 50°, while keeping the oxygen of the carbonyl anchored in the oxyanion hole. As a result of this rotation, the γ-methyl group and the Oγ atom of Thr352, along with the methyl group of the covalently attached acetyl moiety of capsidin, moved inside the active site. Figure 9 shows that the conformational change had a barrier of 2.4 kcal/mol and stabilized the system by 2.9 kcal/mol. As the rotation progressed, the scissile amide bond stretched considerably from 1.56 to 1.67 Å, passing through 1.58 Å at the transition state. At the end of the conformational change, the peptide bond was excessively stretched. The Thr352(Oγ)−(C)capsidin bond shrank from 1.52 to 1.45 Å during this transformation, passing through 1.49 Å at the transition state. To the best of
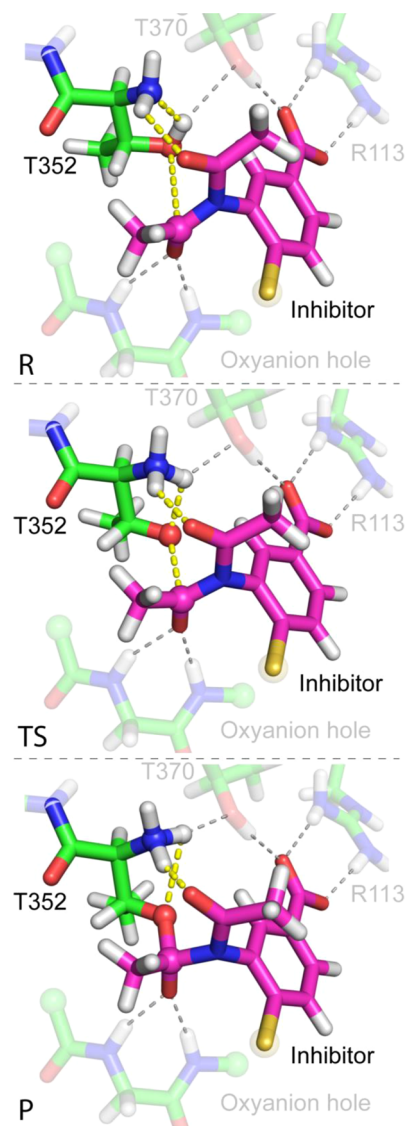

Figure 8. Reactant, transition state, and product for the formation of the tetrahedral intermediate of CapD with covalent inhibitor capsidin. Snapshots of the changes in the QM region of the ONIOM(QM/MM) system along the reaction path. Enzyme carbon atoms are colored green, while inhibitor carbon atoms are colored magenta. Hydrogen, nitrogen, oxygen, and sulfur atoms are colored white, blue, red, and yellow, respectively. Hydrogen bonds between the ligands and the enzyme are shown as dashed gray lines. Dashed yellow lines connect the atoms that are involved in the chemical transformations. The residues of the active site that are not directly involved in the reaction are shown in faded, transparent colors. Atoms that link the QM region to the rest of the system described by molecular mechanics are depicted with transparent spheres around them. These atoms are substituted for hydrogen atoms, and their bond lengths are adjusted accordingly during QM calculations.

our knowledge, this is the first observation of a conformational change directly coupled to covalent enzyme inhibition.

Recently, a structure of the human GGT enzyme that we and others[28,31] have previously homology modeled on the basis of the structure of GGT from *E. coli* was innovatively determined.[25] The high-resolution structure of the human GGT revealed two conformations of the catalytic Thr381 (equivalent to Thr352 in CapD). The authors proposed this feature to be unique to the human GGT and called it a bimodal
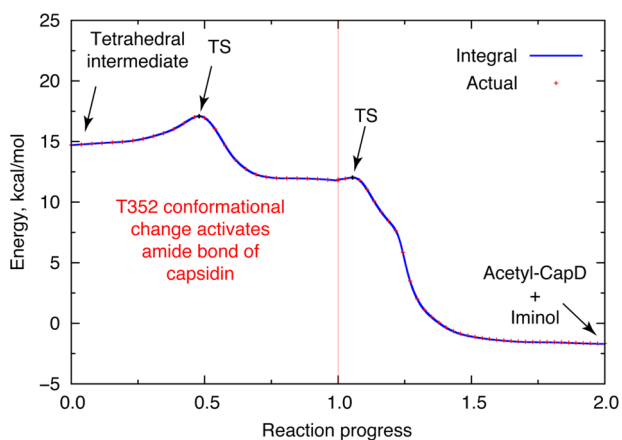
Figure 9. Energy profile for the collapse of the tetrahedral intermediate of CapD with covalent inhibitor capsidin. The energy profile was calculated using the ONIOM[B3LYP/6-31G(d):Amber] potential with electronic embedding and plotted along the reaction path that connects the tetrahedral intermediate to the acetylated CapD with the iminol leaving group of capsidin in two consecutive steps (as parametrized using the reaction progress coordinate). The actual energy levels of the structural snapshots along the reaction are shown with red crosses. The matching integral energy is shown as a solid blue line and was derived from the corresponding forces. The transition states are indicated with black crosses and located atop the corresponding energy peaks. We used 65 system snapshots to generate the energy profile.

switch in the orientation of the catalytic nucleophile. The conformational change in the catalytic Thr352 that was coupled to the scissile amide bond activation in the tetrahedral intermediate of capsidin with bacterial CapD also involved two conformations of the threonine side chain that were nearly identical to those observed in human GGT.

Figures 9 and 11 show yet another unexpected step in the acylation of CapD by capsidin. Specifically, the bottom panel of Figure 11 depicts the corresponding product, acetylated CapD with the unexpected iminol leaving group bound to the donor region of the active site. Figure 11 shows that formation of the iminol involved the transfer of a proton from the N-terminal NH_3^+ group of Thr352 to the carbonyl oxygen of the second acetyl group of the diacetamide moiety of capsidin, rather than to its nitrogen atom. Figure 9 shows that this reaction was essentially barrierless at 0.1 kcal/mol. At the transition state, the already excessively stretched peptide bond was elongated to 1.82 Å before breaking completely. The Thr352(Oγ)−(C)-acetyl bond shrank from 1.45 to 1.32 Å, passing through 1.34 Å at the transition state. The oxyanion hole adjusted slightly to the acetyl group, maintaining the bidentate coordination of the carbonyl. The amide bond of the iminol leaving group settled at 1.28 Å, while the carbonyl bond of the acetyl group shrank from 1.29 to 1.23 Å. The OH group of the iminol formed a hydrogen bond with the N-terminal α-NH_2 group of Thr352.

The process of converting the tetrahedral intermediate of capsidin into acetylated CapD benefited from the presence of the second acetyl group in the inhibitor. In an attempt to rationalize the importance of the second acetyl group, Richter et al. tentatively proposed that it might assist amide bond cleavage via formation of an iminol tautomer.[10] Our calculations corroborated this idea by demonstrating that the second acetyl group of capsidin acted as a "shunt" for formation of the acetylated CapD via the iminol route. Furthermore, our
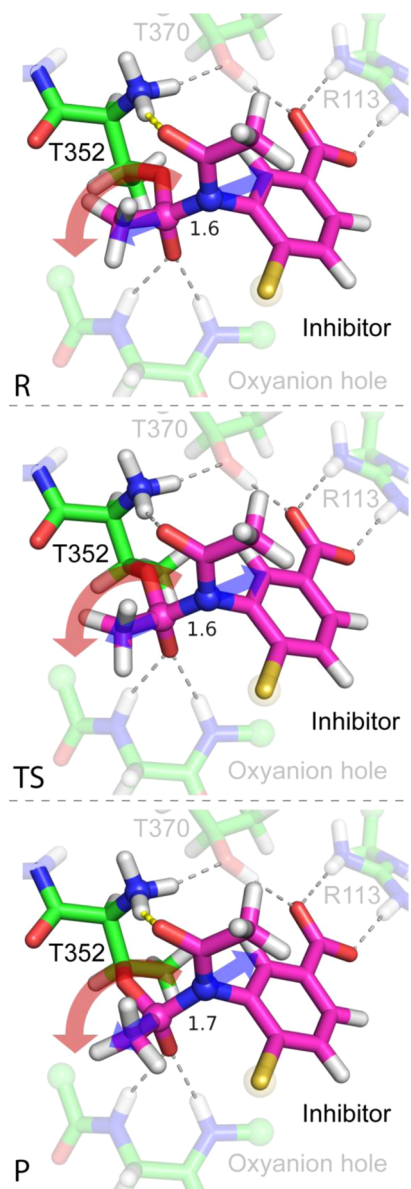

Figure 10. Reactant, transition state, and product for the conformational change of Thr352 coupled to activation of the scissile bond of capsidin in the tetrahedral intermediate of CapD. Shown are snapshots of the changes in the QM region of the ONIOM(QM/MM) system along the reaction path. Enzyme carbon atoms are colored green, while inhibitor carbon atoms are colored magenta. Hydrogen, nitrogen, oxygen, and sulfur atoms are colored white, blue, red, and yellow, respectively. Hydrogen bonds between the ligands and the enzyme are shown as dashed gray lines. Dashed yellow lines connect the atoms that are involved in the chemical transformations. The residues of the active site that are not directly involved in the reaction are shown in faded, transparent colors. Atoms that link the QM region to the rest of the system described by molecular mechanics are depicted with transparent spheres around them. These atoms are substituted for hydrogen atoms, and their bond lengths are adjusted accordingly during QM calculations. The direction of the rotation of the Thr352 side chain is shown with a red transparent arrow. The coupled elongation of the scissile bond is shown with blue transparent arrows.

calculations suggested that binding of the capsidin variant with a single acetyl group at the CapD active site could be catalytically unproductive (see the bottom panel of Figure 12). These observations may help rationalize why derivatives of
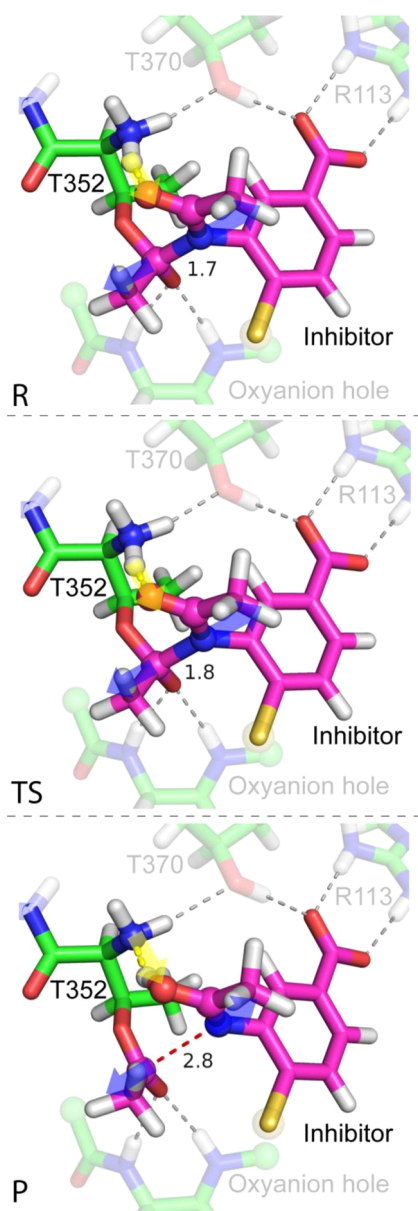
Figure 11. Reactant, transition state, and product for the formation of the acetylated CapD and iminol leaving group of capsidin. Snapshots of the changes in the QM region of the ONIOM(QM/MM) system along the reaction path. Enzyme carbon atoms are colored green, whereas inhibitor carbon atoms are colored magenta. Hydrogen, nitrogen, oxygen, and sulfur atoms are colored white, blue, red, and yellow, respectively. Hydrogen bonds between the ligands and the enzyme are shown as dashed gray lines. Dashed yellow lines connect the atoms that are involved in the chemical transformations. The residues of the active site that are not directly involved in the reaction are shown in faded, transparent colors. Atoms that link the QM region to the rest of the system described by molecular mechanics are depicted with transparent spheres around them. These atoms are substituted for hydrogen atoms, and their bond lengths are adjusted accordingly during QM calculations. The direction of the proton transfer is shown with a yellow transparent arrow. The coupled breaking of the scissile bond is shown with blue transparent arrows.

capsidin lacking the second acetyl group are less potent against CapD.[10]

Iminol versus Amide Leaving Group of Capsidin. Figure 12 shows both iminol and its tautomer amide leaving groups bound to the donor region of the CapD active site. The initial
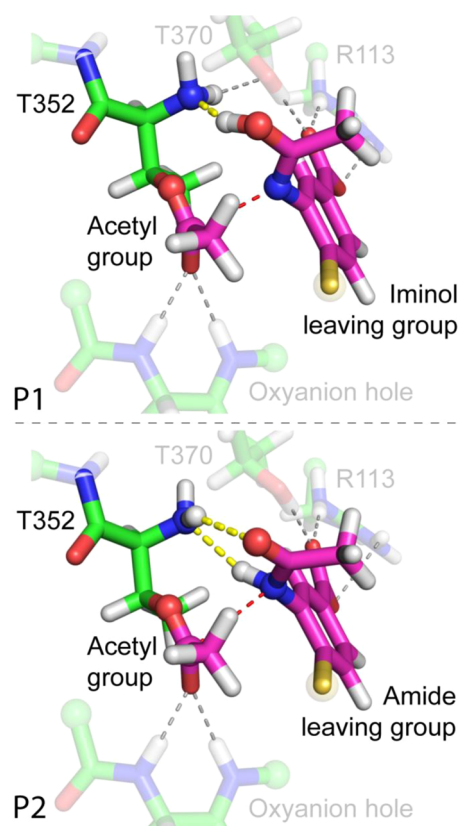

Figure 12. Product of CapD acylation with covalent inhibitor capsidin and two tautomers (iminol and amide) of its leaving group. Structure of the QM region of the ONIOM(QM/MM) system corresponding to the acylated CapD with tautomeric iminol (P1) and amide (P2) leaving groups of capsidin bound to the donor region of the active site. Enzyme carbon atoms are colored green, while carbon atoms of the substrate are colored magenta. Hydrogen, nitrogen, oxygen, and sulfur atoms are colored white, blue, red, and yellow, respectively. Hydrogen bonds between the ligands and the enzyme are shown as dashed gray lines. Dashed yellow lines connect the atoms involved in the chemical transformations. These atoms are also enhanced using solid spheres. The residues of the active site that are not directly involved in the reaction are shown in faded, transparent colors. Atoms that link the QM region to the rest of the system described by molecular mechanics are depicted with transparent spheres around them. These atoms are substituted for hydrogen atoms, and their bond lengths are adjusted accordingly during QM calculations. The dashed red lines connect the atoms of the scissile peptide bond of the inhibitor that has been cleaved.

reaction path for the collapse of the tetrahedral intermediate of CapD was constructed, without any consideration for the iminol, to culminate with the corresponding amide leaving group shown in the bottom panel of Figure 12. Note that the amide leaving group matched one of the variants of capsidin that did not inhibit CapD.[10] The iminol shown in the top panel of Figure 12 was discovered through the optimization of the reaction path. The fact that iminol formation preceded that of the amide and had an extremely low (0.1 kcal/mol) barrier suggested that the iminol group was kinetically more favorable. Furthermore, CapD thermodynamically favored the iminol tautomer over its amide counterpart by 2.9 kcal/mol. The enzyme could catalyze tautomerization of the iminol leaving group into its amide counterpart. However, the barrier for the CapD-mediated tautomerization was estimated to be around 22 kcal/mol.
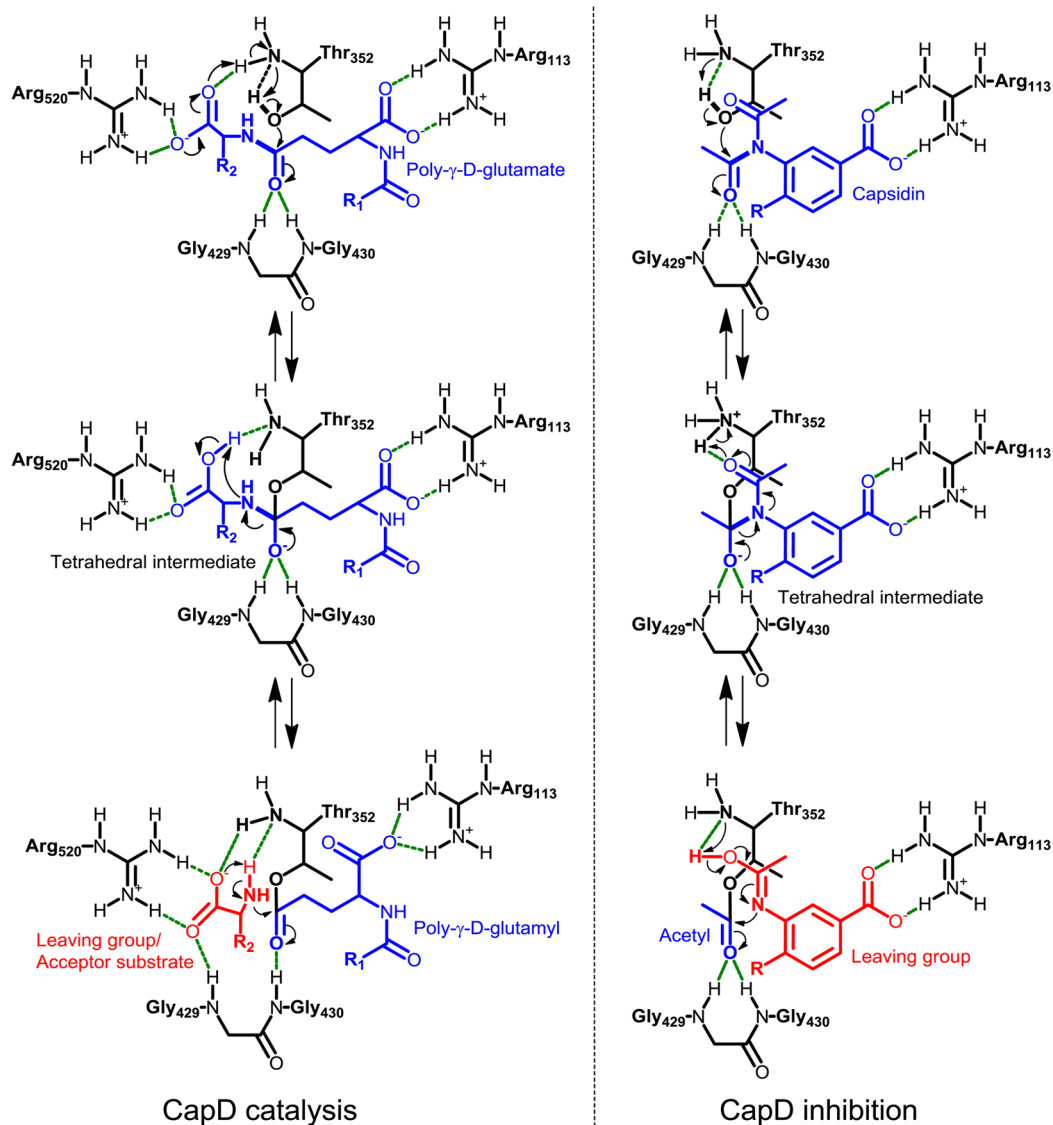
Figure 13. Summary of the calculated mechanism of catalysis and inhibition of CapD. CapD active site residues are colored black, whereas the poly-γ-D-glutamate substrate and capsidin inhibitor are colored blue. The hydrogen bonds are shown as dashed green lines. The scissile peptide bonds of the substrate and inhibitor are highlighted with thick solid lines. Upon cleavage of the scissile peptide bond, the resulting leaving group is colored red, while the covalently attached acyl group is colored blue. Curved arrows illustrate the proposed movement of electrons.

Can the collapse of the tetrahedral intermediate of CapD with capsidin bypass the iminol and form an amide leaving group directly? Hypothetically, amide formation could start from the initial tetrahedral intermediate or from its variant with the activated scissile bond (R or P in Figure 10, respectively). Each state has a relatively strong hydrogen bond between the carbonyl of the capsidin leaving group and the α-amine of Thr352. This hydrogen bond was involved in iminol formation. Without breaking this hydrogen bond, another proton of the α-amine would need to transfer to the amide nitrogen over a much larger distance. Because the distance is much shorter in the activated tetrahedral intermediate, we consider only reaction paths that start from the activated intermediate. The barrier for iminol formation from the activated tetrahedral intermediate is only 0.1 kcal/mol, and the only way formation of the amide could bypass iminol would be if it had a comparable barrier.

Promiscuity of CapD in the Consideration of Drug Design. Enzyme promiscuity can be exploited to design irreversible inhibitors of CapD. The donor region of the active site was an unusual place for a leaving group to bind, because the donor region typically bound the γ-glutamyl moiety that covalently attached to Thr352 of CapD. In the case of capsidin, it was a small acetyl group that covalently attached to Thr352, in agreement with experimental observations.[10] Because of the lack of other functional groups, the acetyl group could bind the oxyanion hole only in the central region of the active site of CapD.

In the absence of functional groups that could bind the donor region of the active site, the acyl group of the inhibitor that covalently attaches to the catalytic Thr352 may be displaced from the oxyanion hole and form a hydrogen bond with the α-amine of Thr352 instead. Such a conformation of the acyl-CapD intermediate is not conducive to hydrolysis or transpeptidation and could lead to irreversible inhibition of the enzyme. Therefore, designing covalent inhibitors that position their scissile amide bond in the donor rather than acceptor

region of the active site of CapD could be a viable strategy for irreversible inhibition.

In conclusion, our study of CapD inhibition with capsidin suggested that formation of the corresponding tetrahedral intermediate was the rate-limiting step. Overall, the acetylation of CapD was 1.7 kcal/mol exothermic with the iminol leaving group. Unlike with diDGA, the α-amino group of Thr352 was protonated in the metastable tetrahedral intermediate of capsidin. In agreement with experimental observations, the acetylated CapD was predicted to be a stable intermediate.

■ CONCLUSIONS

This study demonstrates just how promiscuous the CapD enzyme really is. Starting with the prereaction complex, CapD binds diDGA and capsidin in two very different ways, as summarized in Figure 13. The differences pertain to the side (*Re* or *Si*) of the scissile amide bond that faces the nucleophilic Thr352 residue or, alternatively, the region of the active site (acceptor or donor) that contains the scissile bond. The scissile amide bond of diDGA is in the acceptor region of the active site, whereas that of capsidin is in the donor region of the active site of CapD. This orientation determines which region of the active site, i.e., donor versus acceptor, will contain the leaving group upon formation of the acylated CapD. Therefore, shifting the position of the scissile bond within the molecule could be used to design new irreversible inhibitors of CapD.

Figure 13 shows that even though the formations of the tetrahedral intermediates from diDGA and capsidin were both initiated with an unprotonated α-amine of Thr352 and had similar energy barriers, the two processes were quite different. The diDGA substrate assisted in formation of the tetrahedral intermediate, using the carboxyl group that was adjacent to the scissile γ-peptide bond. As a result, the formation of the tetrahedral intermediate was a double-proton-coupled concerted asynchronous reaction. The catalytic Thr352 was only protonated during a small part of the reaction progress, essentially just relaying the proton to the carboxyl group of diDGA. In contrast, the reaction with capsidin involved a single proton transfer. This resulted in the protonated α-amine of Thr352 being associated with the capsidin tetrahedral intermediate. This tetrahedral intermediate was significantly more stable (14.7 kcal/mol) than that of diDGA (18.0 kcal/mol). However, none of these tetrahedral intermediates would be stable enough to be experimentally observed.

The ways the two tetrahedral intermediates were converted into the acylated CapD were also quite different. Uniquely, capsidin involved a prerequisite step during which a conformational change, i.e., rotation about the $C\alpha-C\beta$ bond of Thr352, was coupled to an excessive stretching of the scissile amide bond, i.e., activation of the scissile bond for cleavage. This step greatly facilitated subsequent proton transfer and collapse of the tetrahedral intermediate.

The tetrahedral intermediate of diDGA could collapse by transferring its proton from the protonated carboxyl to the nitrogen of the scissile peptide bond in four consecutive steps. The highest energy barrier for the collapse was found to be 10.0 kcal/mol. It is also possible that water molecules could mediate the proton transfer. In contrast, the tetrahedral intermediate of capsidin exploited the second acetyl group and transferred the proton directly from the α-NH_3^+ group of Thr352 to the oxygen of the acetyl group in two consecutive steps. The highest energy barrier for the collapse was found to be 2.4 kcal/mol. This transition yielded an iminol leaving group that could

subsequently tautomerize to the corresponding amide. The leaving group of capsidin was bound to the donor region of the CapD active site.

In contrast to capsidin, the leaving group of diDGA was bound to the acceptor region of the active site. Moreover, the leaving group of diDGA demonstrated how an acceptor substrate might bind CapD during the transpeptidation catalytic cycle.[31] The product of CapD acylation with diDGA also revealed that the oxyanion hole could bind both the acceptor substrate and the transferring γ-glutamyl simultaneously. The amino group of the substrate that accepts the γ-glutamyl and that of the Thr352 were both deprotonated. The barrier for the first step of transpeptidation was estimated to be at least as high as the barrier for formation of the tetrahedral intermediate.

■ ASSOCIATED CONTENT

ⓢ Supporting Information

A detailed description of the non-rate-limiting collapse of the tetrahedral intermediate of CapD with pDGA and with capsidin along with the corresponding tables and figures summarizing the energy and structural changes. This material is available free of charge via the Internet at http://pubs.acs.org.

■ AUTHOR INFORMATION

Corresponding Author

*E-mail: ikhavrutskii@bhsai.org.

■ ACKNOWLEDGMENTS

■ REFERENCES

(1) Spencer, R. C. (2003) *Bacillus anthracis. J. Clin. Pathol. 56* (3), 182−187.

(2) Martin, G. J., and Friedlander, A. M. (2010) *Bacillus anthracis* (Anthrax). In *Principles and Practices of Infectious Diseases* (Mandell, G. L., Bennett, J. E., and Dolin, R., Eds.) Vol. 2, pp 2715−2725, Churchill Livingstone, Philadelphia.

(3) Smith, H., Keppie, J., and Stanley, J. L. (1953) The Chemical Basis of the Virulence of *Bacillus anthracis.* I: Properties of Bacteria Grown in vivo and Preparation of Extracts. *Br. J. Exp. Pathol. 34* (5), 477−485.

(4) Keppie, J., Harris-Smith, P. W., and Smith, H. (1963) The Chemical Basis of the Virulence of *Bacillus anthracis* IX. Its Aggressins and Their Mode of Action. *Br. J. Exp. Pathol. 44* (4), 446−453.

(5) Makino, S.-I., Uchida, I., Terakado, N., Sasakawa, C., and Yoshikawa, M. (1989) Molecular Characterization and Protein Analysis of the Cap Region, Which Is Essential for Encapsulation in *Bacillus anthracis. J. Bacteriol. 171* (2), 722−730.

(6) Scorpio, A., Chabot, D. J., Day, W. A., O'Brien, D. K., Vietri, N. J., Itoh, Y., Mohamadzadeh, M., and Friedlander, A. M. (2007) Poly-γ-glutamate Capsule-Degrading Enzyme Treatment Enhances Phag-

ocytosis and Killing of Encapsulated *Bacillus anthracis*. *Antimicrob. Agents Chemother. 51* (1), 215−222.

(7) Ezzell, J. W., Abshire, T. G., Panchal, R., Chabot, D., Bavari, S., Leffel, E. K., Purcell, B., Friedlander, A. M., and Ribot, W. J. (2009) Association of *Bacillus anthracis* Capsule with Lethal Toxin during Experimental Infection. *Infect. Immun. 77* (2), 749−755.

(8) Fouet, A. (2009) The Surface of *Bacillus anthracis*. *Mol. Aspects Med. 30* (6), 374−385.

(9) Candela, T., and Fouet, A. (2006) Poly-γ-glutamate in Bacteria. *Mol. Microbiol. 60* (5), 1091−1098.

(10) Richter, S., Anderson, V. J., Garufi, G., Lu, L., Budzik, J. M., Joachimiak, A., He, C., Schneewind, O., and Missiakas, D. (2009) Capsule Anchoring in *Bacillus anthracis* Occurs by a Transpeptidation Reaction that is Inhibited by Capsidin. *Mol. Microbiol. 71* (2), 404−420.

(11) Oinonen, C., and Rouvinen, J. (2000) Structural Comparison of Ntn-Hydrolases. *Protein Sci. 9* (12), 2329−2337.

(12) Uchida, I., Makino, S.-I., Sasakawa, C., Yoshikawa, M., Sugimoto, C., and Terakado, N. (1993) Identification of a novel gene, *dep*, associated with depolymerization of the capsular polymer in *Bacillus anthracis*. *Mol. Microbiol. 9* (3), 487−496.

(13) Bokhove, M., Jimenez, P. N., Quax, W. J., and Dijkstra, B. W. (2010) The Quorum-Quenching N-Acyl Homoserine Lactone Acylase PvdQ Is an Ntn-Hydrolase With an Unusual Substrate-Binding Pocket. *Proc. Natl. Acad. Sci. U.S.A. 107* (2), 686−691.

(14) Zhiryakova, D., Ivanov, I., Ilieva, S., Guncheva, M., Galunsky, B., and Stambolieva, N. (2009) Do N-Terminal Nucleophile Hydrolases Indeed Have a Single Amino Acid Catalytic Center? Supporting Amino Acid Residues at the Active Site of Penicilin G Acylase. *FEBS J. 276* (9), 2589−2598.

(15) Chilov, G. G., Sidorova, A. V., and Svedas, V. K. (2007) Quantum Chemical Studies of the Catalytic Mechanism of N-Terminal Nucleophile Hydrolase. *Biochemistry (Moscow) 72* (5), 495−500.

(16) Perakyla, M., and Kollman, P. A. (1997) A Simulation of the Catalytic Mechanism of Aspartylglucosaminidase Using ab Initio Quantum Mechanics and Molecular Dynamics. *J. Am. Chem. Soc. 119* (6), 1189−1196.

(17) Perakyla, M., and Rouvinen, J. (1996) Ab Initio Quantum Mechanical Model Calculations on the Catalytic Mechanism of Aspartylglucosaminidase (AGA): A Serine Protease-Like Mechanism with an N-Terminal Threonine and Substrate-Assisted Catalysis. *Chem.—Eur. J. 2* (12), 1548−1551.

(18) Guidi-Rontani, C., Weber-Levy, M., Labruyere, E., and Mock, M. (1999) Germination of *Bacillus anthracis* Spores within Alveolar Macrophages. *Mol. Microbiol. 31* (1), 9−17.

(19) Langer, M., Duggan, E. S., Booth, J. L., Patel, V. I., Zander, R. A., Silasi-Mansat, R., Ramani, V., Veres, T. Z., Prenzler, F., Sewald, K., Williams, D. M., Coggeshall, K. M., Awasthi, S., Lupu, F., Burian, D., Ballard, J. D., Braun, A., and Metcalfa, J. P. (2012) *Bacillus anthracis* Lethal Toxin Reduces Human Alveolar Epithelial Barrier Function. *Infect. Immun. 80* (12), 4374−4387.

(20) Scorpio, A., Tobery, S. A., Ribot, W. J., and Friedlander, A. M. (2008) Treatment of Experimental Anthrax with Recombinant Capsule Depolymerase. *Antimicrob. Agents Chemother. 52* (3), 1014−1020.

(21) Scorpio, A., Chabot, D. J., Day, W. A., Hoover, T. A., and Friedlander, A. M. (2010) Capsule Depolymerase Overexpression Reduces *Bacillus anthracis* Virulence. *Microbiology 156* (5), 1459−1467.

(22) Wu, S. J., Eiben, C. B., Carra, J. H., Huang, I., Zong, D., Liu, P., Wu, C. T., Nivala, J., Dunbar, J., Huber, T., Senft, J., Schokman, R., Smith, M. D., Mills, J. H., Friedlander, A. M., Baker, D., and Siegel, J. B. (2011) Improvement of a Potential Anthrax Therapeutic by Computational Protein Design. *J. Biol. Chem. 286* (37), 32586−32592.

(23) Lodola, A., Branduardi, D., De Vivo, M., Capoferri, L., Mor, M., Piomelli, D., and Cavalli, A. (2012) A Catalytic Mechanism for Cysteine N-Terminal Nucleophile Hydrolases, as Revealed by Free Energy Simulations. *PLoS One 7* (2), e32397.

(24) Morrow, A. L., Williams, K., Sand, A., Boanca, G., and Barycki, J. J. (2007) Characterization of *Helicobacter pylori* γ-Glutamyltranspeptidase Reveals the Molecular Basis for Substrate Specificity and a Critical Role for the Tyrosine 433-Containing Loop in Catalysis. *Biochemistry 46* (46), 13407−13414.

(25) West, M. B., Chen, Y., Wickham, S., Heroux, A., Cahill, K., Hanigan, M. H., and Mooers, B. H. M. (2013) Novel Insights into Eukaryotic γ-Glutamyltranspeptidase 1 from the Crystal Structure of the Glutamate-bound Human Enzyme. *J. Biol. Chem. 288* (44), 31902−31913.

(26) Wada, K., Irie, M., Suzuki, H., and Fukuyama, K. (2010) Crystal Structure of the Halotolerant γ-Glutamyltranspeptidase from *Bacillus subtilis* in Complex with Glutamate Reveals a Unique Architecture of the Solvent-Exposed Catalytic Pocket. *FEBS J. 277* (4), 1000−1009.

(27) Wada, K., Hiratake, J., Irie, M., Okada, T., Yamada, C., Kumagai, H., Suzuki, H., and Fukuyama, K. (2008) Crystal Structures of *Escherichia coli* γ-Glutamyltranspeptidase in Complex with Azaserine and Acivicin: Novel Mechanistic Implication for Inhibition by Glutamine Antagonists. *J. Mol. Biol. 380* (2), 361−372.

(28) Boanca, G., Sand, A., Okada, T., Suzuki, H., Kumagai, H., Fukuyama, K., and Barycki, J. J. (2007) Autoprocessing of *Helicobacter pylori* γ-Glutamyltranspeptidase Leads to the Formation of a Threonine-Threonine Catalytic Dyad. *J. Biol. Chem. 282* (1), 534−541.

(29) Wu, R., Richter, S., Zhang, R.-G., Anderson, V. J., Missiakas, D., and Joachimiak, A. (2009) Crystal Structure of *Bacillus anthracis* Transpeptidase Enzyme CapD. *J. Biol. Chem. 284* (36), 24406−24414.

(30) Okada, T., Suzuki, H., Wada, K., Kumagai, H., and Fukuyama, K. (2006) Crystal Structures of γ-Glutamyltranspeptidase from *Escherichia coli*, a Key Enzyme in Glutathione Metabolism, and Its Reaction Intermediate. *Proc. Natl. Acad. Sci. U.S.A. 103* (17), 6471−6476.

(31) Hu, X., Legler, P. M., Khavrutskii, I. V., Scorpio, A., Compton, J. R., Robertson, K. L., Friedlander, A. M., and Wallqvist, A. (2012) Probing the Donor and Acceptor Substrate Specificity of the γ-Glutamyl Transpeptidase. *Biochemistry 51* (6), 1199−1212.

(32) Trott, O., and Olson, A. J. (2010) AutoDock Vina: Improving the Speed and Accuracy of Docking with a New Scoring Function, Efficient Optimization, and Multithreading. *J. Comput. Chem. 31* (2), 455−461.

(33) Khavrutskii, I. V., Smith, J. B., and Wallqvist, A. (2013) Exploring Chemical Reaction Mechanisms through Harmonic Fourier Beads Path Optimization. *J. Chem. Phys. 139* (16), 165104.

(34) Svensson, M., Humbel, S., Froese, R. D. J., Matsubara, T., Sieber, S., and Morokuma, K. (1996) ONIOM: A Multilayered Integrated MO+MM Method for Geometry Optimizations and Single Point Energy Predictions. A Test for Diels-Alder Reactions and Pt(P(t-Bu)$_3$)$_2$ + H$_2$ Oxidative Addition. *J. Phys. Chem. 100* (50), 19357−19363.

(35) Dapprich, S., Komaromi, I., Byun, K. S., Morokuma, K., and Frisch, M. J. (1999) A New ONIOM Implementation in Gaussian98. Part I. The Calculation of Energies, Gradients, Vibrational Frequencies and Electric Field Derivatives. *J. Mol. Struct.: THEOCHEM 461*, 1−21.

(36) Vreven, T., Byun, K. S., Komaromi, I., Dapprich, S., Montgomery, J. A., Morokuma, K., and Frisch, M. J. (2006) Combining Quantum Mechanics Methods with Molecular Mechanics Methods in ONIOM. *J. Chem. Theory Comput. 2* (3), 815−826.

(37) Carter, P., and Wells, J. A. (1987) Engineering Enzyme Specificity by "Substrate-Assisted Catalysis". *Science 237* (4813), 394−399.

(38) Dennington, R., Keith, T., and Millam, J. (2009) *GaussView*, version 5, Semichem Inc., Shawnee Mission, KS.

(39) Cornell, W. D., Cieplak, P., Bayly, C. I., Gould, I. R., Merz, K. M., Ferguson, D. M., Spellmeyer, D. C., Fox, T., Caldwell, J. W., and Kollman, P. A. (1995) A Second Generation Force Field for the Simulation of Proteins, Nucleic Acids, and Organic Molecules. *J. Am. Chem. Soc. 117* (19), 5179−5197.

(40) Wang, J. (2009) *Antechamber*, version 1.2, Amber Software, San Francisco.

(41) Wang, J., Wang, W., Kollman, P. A., and Case, D. A. (2006) Automatic Atom Type and Bond Type Perception in Molecular Mechanical Calculations. *J. Mol. Graphics Modell.* 25 (2), 247−260.

(42) Frisch, M. J., Trucks, G. W., Schlegel, H. B., Scuseria, G. E., Robb, M. A., Cheeseman, J. R., Scalmani, G., Barone, V., Mennucci, B., Petersson, G. A., Nakatsuji, H., Caricato, M., Li, X., Hratchian, H. P., Izmaylov, A. F., Bloino, J., Zheng, G., Sonnenberg, J. L., Hada, M., Ehara, M., Toyota, K., Fukuda, R., Hasegawa, J., Ishida, M., Nakajima, T., Honda, Y., Kitao, O., Nakai, H., Vreven, T., Montgomery, J. A., Jr., Peralta, J. E., Ogliaro, F., Bearpark, M., Heyd, J. J., Brothers, E., Kudin, K. N., Staroverov, V. N., Kobayashi, R., Normand, J., Raghavachari, K., Rendell, A., Burant, J. C., Iyengar, S. S., Tomasi, J., Cossi, M., Rega, N., Millam, J. M., Klene, M., Knox, J. E., Cross, J. B., Bakken, V., Adamo, C., Jaramillo, J., Gomperts, R., Stratmann, R. E., Yazyev, O., Austin, A. J., Cammi, R., Pomelli, C., Ochterski, J. W., Martin, R. L., Morokuma, K., Zakrzewski, V. G., Voth, G. A., Salvador, P., Dannenberg, J. J., Dapprich, S., Daniels, A. D., Farkas, Ö., Foresman, J. B., Ortiz, J. V., Cioslowski, J., and Fox, D. J. (2009) *Gaussian 09*, revision A.1, Gaussian Inc., Wallingford, CT.

(43) Wolynes, P. G., Onuchic, J. N., and Thirumalai, D. (1995) Navigating the Folding Routes. *Science* 267 (5204), 1619−1620.

(44) Dill, K. A., and Chan, H. S. (1997) From Levinthal to Pathways to Funnels. *Nat. Struct. Mol. Biol.* 4 (1), 10−19.

(45) Dewar, M. J. S., Zoebisch, E. G., Healy, E. F., and Stewart, J. J. P. (1985) AM1: A New General Purpose Quantum Mechanical Molecular Model. *J. Am. Chem. Soc.* 107 (13), 3902−3909.

(46) Vreven, T., and Morokuma, K. (2006) in *Hybrid Methods: ONIOM(QM:MM) and QM/MM* (Spellmeyer, D. C., Ed.) Vol. 2, pp 35−51, Elsevier, Oxford, U.K.

(47) Vreven, T., Morokuma, K., Farkas, O., Schlegel, H. B., and Frisch, M. J. (2003) Geometry Optimization with QM/MM, ONIOM, and Other Combined Methods. I. Microiterations and Constraints. *J. Comput. Chem.* 24 (6), 760−769.

(48) Avinash, V. S., Panigrahi, P., Suresh, C. G., Pundle, A. V., and Ramasamy, S. (2013) Structural Modelling of Substrate Binding and Inhibition in Penicillin V Acylase from *Pectobacterium atrosepticum*. *Biochem. Biophys. Res. Commun.* 437 (4), 538−543.

(49) Adediran, S. A., Lin, G., Pelto, R. B., and Pratt, R. F. (2012) Crossover Inhibition as an Indicator of Convergent Evolution of Enzyme Mechanisms: A β-Lactamase and an N-Terminal Nucleophile Hydrolase. *FEBS Lett.* 586 (23), 4186−4189.

(50) Buller, A. R., and Townsend, C. A. (2013) Intrinsic Evolutionary Constraints on Protease Structure, Enzyme Acylation, and the Identity of the Catalytic Triad. *Proc. Natl. Acad. Sci. U.S.A.* 110 (8), E653−E661.

(51) Low, P. S., Bada, J. L., and Somero, G. N. (1973) Temperature Adaptation of Enzymes: Roles of the Free Energy, the Enthalpy, and the Entropy of Activation. *Proc. Natl. Acad. Sci. U.S.A.* 70 (2), 430−432.

(52) McVey, C. E., Walsh, M. A., Dodson, G. G., Wilson, K. S., and Brannigan, J. A. (2001) Crystal Structures of Penicillin Acylase Enzyme-Substrate Complexes: Structural Insights into the Catalytic Mechanism. *J. Mol. Biol.* 313 (1), 139−150.

(53) Duggleby, H. J., Tolley, S. P., Hill, C. P., Dodson, E. J., Dodson, G. G., and Moody, P. C. E. (1995) Penicillin Acylase Has a Single-Amino-Acid Catalytic Centre. *Nature* 373 (6511), 264−268.

(54) Alkema, W. B. L., Hensgens, C. M. H., Kroezinga, E. H., de Vries, E., Floris, R., van der Laan, J.-M., Dijkstra, B. W., and Janssen, D. B. (2000) Characterization of β-Lactam Binding Site of Penicilin Acylase of *Escherichia coli* by Structural and Site-Directed Mutagenesis Studies. *Protein Eng.* 13 (12), 857−863.

(55) Morelli, C. F., Calvio, C., Biagiotti, M., and Speranza, G. (2014) pH-Dependent Hydrolase, Glutaminase, Transpeptidase and Auto-transpeptidase Activities of *Bacillus subtilis* γ-Glutamyltransferase. *FEBS J.* 281 (1), 232−245.

(56) Balakrishna, S., and Prabhune, A. (2014) Effect of pH on the Hydrolytic Kinetics of γ-Glutamyl Transferase from *Bacillus subtilis*. *Sci. World J.* 2014, 6.